Laser micro-machining of sharp edged receptor sites in polyimide for fluid driven self-alignment

G.R.B.E RÖMER[*1], D. ARNALDO DEL CERRO[*1], M. JORRITSMA[*1], R. POHL[*1], B. CHANG[*2], V. LIIMATAINEN[*2], Q. ZHOU[*2] and A.J. HUIS IN 'T VELD[*1,3]

[*1] *University of Twente, Faculty of Engineering Technology, Chair of Applied Laser Technology, Drienerlolaan 5, 7522 NB, Enschede, The Netherlands*
E-mail: g.r.b.e.romer@utwente.nl
[*2] *Aalto University, Electrical Engineering, Department of Automation and Systems Technology, 00076 Aalto, Finland*
[*3] *TNO Mechatronics, Mechanics and Materials, De Rondom 1, 5600 HE, Eindhoven, The Netherlands*

Fluidic self-alignment of micro-fabricated components, e.g. semiconductor dies, is based on a locally confined liquid droplet (e.g. water) on top of which the component is "dropped". In this approach, capillary action provides the driving force for self-alignment of the component. The ability of a receptor site to pin/confine the droplet depends on three key factors: (*i*) the chemical composition of the surface, (*ii*) its roughness, as well as (*iii*) geometrical features, such as edges, that are able to stop the advancing of a liquid front. According to Gibbs' inequality, the sharper the edge of a geometrical feature, the more it will impede the liquid from advancing. In prior work, on a metallic substrate, a pico-second pulsed laser source was used to machine "trenches" around a receptor site, exploiting the third factor to confine the droplet. However, the edge angles of these trenches were limited to about 100º at best. Moreover, the volume of the liquid that could be pinned was limited due the initial high roughness of the substrate. The work reported in this paper addresses both issues, by taking advantage of a polyimide foil as a substrate material. Trenches of about 25µm wide around sites of about 200×200µm^2 were machined employing a pico-second pulsed laser source at a wavelength of 343nm. It was found that sharp edges up to about 95º could be readily created. Near the edges of the trenches, "dents" and "humps" were found, which could be attributed to amorphization or due to fragmentation of polymer chains at fluence levels just below the ablation threshold. The humps show steep edge angles, which provide a suitable geometrical feature to stop the advancing of the liquid. In addition, it was confirmed experimentally, by a video based optical measurement setup, that the volume of the droplet that can be pinned on the receptor site increases with increasing edge angle. Also, it was found, by using a robotic micro-assembly system that, a 100% success rate of self-alignment of SU-8 parts on the receptor sites can be achieved.

Keywords: Laser, Ultra short laser pulse, hydropobic/hydrophilic patterning, self-alignment

1. Introduction

Fluid driven self-alignment is a low cost alternative to fast, but relatively inaccurate robotic pick-and-place assembly of micro-fabricated components [1,2]. For example in 3D integration of functional components, such as IC's, into highly integrated micro- and nano-systems [2]. The fluidic self-alignment technique relies on a hydrophobic/hydrophilic pattern on the surface of the receiving substrate, which confines the fluid to a receptor site (Figure 1b). Releasing a micro-component of typically 100×100 µm^2 on the fluid (Figure 1c and d), capillary forces drive the alignment of the part to the receptor site (Figure 1e) [2]. Optimizing the shapes, and the relative wetting properties of both the receptor site and the part, this self-alignment

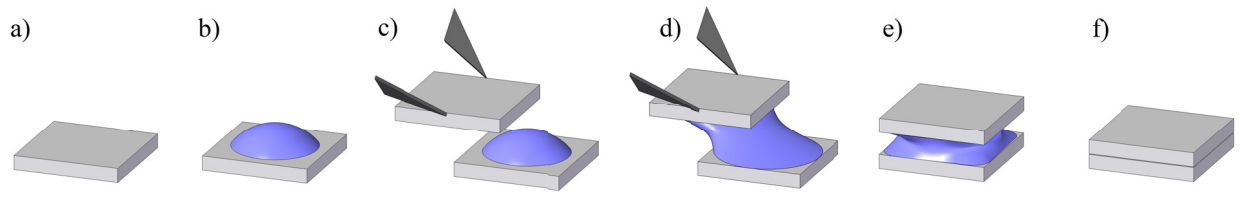

Fig. 1 Fluid driven self-alignment: (a) Receptor site, (b) a droplet of a liquid is dispensed on the receptor site, (c) a gripper approaches the site with a part, (d) the part contacts with the droplet, (e) the gripper releases the part and the capillary force aligns the parts, (f) the liquid between the two parts evaporates, which leaves the two parts aligned [2].

technique allows for accurate positioning (about ±2 μm) of the part to the receptor site (Figure 1f). Angluar accuracies of typically ±0.5° have been reported [2,3]. Moreover, it was shown, that capillary forces can overcome initial positioning errors (Figure 1d) of up to 180μm in the case of a part of 300×300μm^2 [4,5].

As was discussed in an earlier publication [6], the ability of a receptor site to pin/confine the droplet depends on three key factors:

i. the chemical composition of the surface of the substrate, and
ii. its topography, which can be subdivided into two factors related to:
    a. roughness or texture, of the surface, and
    b. geometrical features, such as edges, that are able to stop the advancing of a liquid front.

It was shown that, factor ii.b can be efficiently and effectively exploited when applying an Ultra Short Pulsed Laser (USPL) source [6]. That is, well-defined edges around the receptor site can be created by selectively removing material from the perimeter of the receptor site, by laser ablation, see Figure 2. This approach is suitable for both hydrophobic and hydrophilic substrates and is therefore, more flexible than the alternative approaches i. and ii.a, listed above.

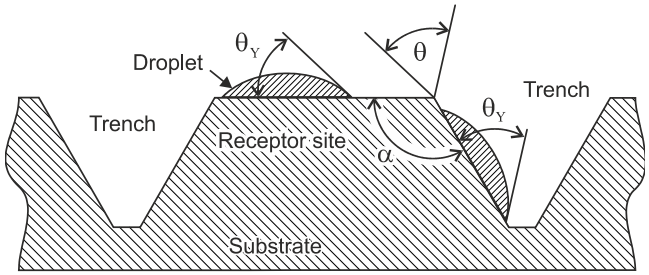

Fig. 2 An receptor site can be created by removing material (by laser ablation) from the tracks of a laser path that follows the perimeter of the site. The sharper angle α of the edge of the resulting trench, the more it will impede the liquid front from crossing the edge.

The edges of the tracks will provide a location for the pining of the liquid-solid-vapour interface of a droplet. It has been shown [7,8] that the sharper the angle α [deg] of an edge the more it will impede the liquid front from crossing the modified perimeter, see Figure 2. The latter is described by Gibbs condition,

$$\theta_Y<\theta<(180-\alpha)+\theta_Y \qquad (1)$$

were θ_Y [deg] is Young's equilibrium contact angle, which a droplet adopts when in contact with a flat/smooth surface [9,10]. It follows from this inequality that a large local contact angle θ [deg] will be formed before a liquid front overflows an edge/obstacle with a small edge angle α, see Figure 2. Sharp edges (with small values of α) can be accurately machined by a proper selection of the laser processing parameters.

The feasibility and performance of fluidic self-alignment has been shown on metallic substrate [6]. In this paper a polymer, popular in the field of electronics, is studied as the base material.

2. Scope of this paper

Section 3 discusses the material and experimental set-up. Next, in section 4, the laser processing conditions are discussed to obtain sharp edged receptor sites. This section also presents the capability of those sites the pin a water droplet, as well as the self-alignment performance, as a function of the edge angle. Finally, conclusions are given in section 5.

3. Material and experimental setup

3.1 Material

The substrate under consideration is polyimide (PI). This polymer is applied frequently in electronics applications, and is known for its electrical, thermal, chemical and mechanical properties. Its applications are found in a range of industries including consumer electronics, solar photovoltaic and wind energy, aerospace, automotive and industrial applications. The thickness of the PI foil applied was 25±2 μm. To allow handling, the foil was fixed on a copper sheet of about 230 μm thickness. The substrate was cleaned ultrasonically in isopropanol prior to, as well as after, laser machining.

The surface topography of the machined surfaces was analyzed by a Confocal Laser Scanning Microscope (CLSM), type VK-9700, of KEYENCE, Osaka, Japan.

3.2 Laser setup

An Yb:YAG laser source, type TRUMICRO 5050 of TRUMPF GMBH, Germany, with a central wavelength of 1030 nm (IR) was used for generation of the laser pulses. But for the experiments, a Third Harmonic Generation (THG) unit was applied to convert the central wavelength to 343nm (UV), as the absorption of laser energy of the substrate at this wavelength is higher than at IR. Moreover, the UV wavelength, in contrast to the IR wavelength, allows for focusing the laser beam into a smaller diameter, which, in turn, facilitates machining of smaller and more accurate features. The beam shows a nearly Gaussian power density profile (M^2<1.3). The pulse duration was constant at 6.7ps for all experiments. The radiation was linearly polarized.

Manipulation of the beam over the samples was accomplished by a two mirror Galvano-scanner system, type INTELLISCAN14 of SCANLAB GMBH, of Puchheim, Germany. A telecentric 100 mm fθ-lens, type RONAR of LINOS GMBH, of Göttingen, Germany, focused the beam. The substrate was irradiated at normal incidence at environmental conditions.

3.3 Set-up for liquid pinning & self-alignment tests

A microassembly system was used to carry out liquid confinement (pinning) tests, as well as self-alignment tests [2]. The system includes a robotic microgripper, two microscopes, three motorized stages and a droplet dispenser. The microgripper is custom built, driven by two piezoelectric benders. The motorized stages provide movement in *x*-,*y*-

and *z*-directions. The *z*-axis stage (type M-122.2DD of PHYSIK INSTRUMENTE, Karlsruhe, Germany) moves the microgripper vertically, while the *x*-axis stage (type M-122.2DD of PHYSIK INSTRUMENTE) and y-axis stage (type M-404.8PD of PHYSIK INSTRUMENTE) move the test patterns (leadframe) horizontally. The droplet dispenser (type PicPIP of GESIM, Grosserkmannsdorf, Germany) is non-contact type, actuated by a piezoelectric diaphragm. It can dispense droplets in a distance of a few millimeters with a resolution of tens of pico-liters depending on the control parameters.

The self-alignment process was imaged from a top view microscope (type VZM1000i of EDMUND, Nether Poppleton, UK) and a side view microscope (type VZM1000i, EDMUND). A high-speed CMOS video camera (type IPX-VGA210-G of IMPERX of Boca Raton, USA) was attached to the top microscope and a CCD video camera (type SCA1600-14GC of BASLER, Ahrensburg, Germany) has been attached to the side view microscope.

4. Results and discussions

Measurements, using the CLSM, showed that the surface roughness of the PI, prior to laser machining, was $R_a \approx 0.04\mu m$. It is known from earlier work [6] that, for successful fluidic self-alignment, the trench depth shall be larger than this roughness.

4.1 Ablation threshold

The ablation threshold, or more specifically the fluence threshold, above which the substrate under laser radiation, will be ablated, was determined using a method usually referred to as the *D^2-method* [11-13]. Besides the ablation threshold, this methods yields also the beam diameter. The latter was found to equal 15.6 µm. The ablation threshold was found to equal 0.06 J/cm^2.

4.2 Processing conditions for single laser tracks

Next, laser machining conditions were experimentally determined to create trenches in the substrate. To ensure a uniform depth along the length of the trench, the pulse-to-pulse overlap (OL) was chosen relatively high. To this end, as well as to ensure a relatively high machining rate, the velocity of the focal spot relative to the substrate was set to v=400 mm/s. The pulse frequency was fixed at the maximum of the laser source at f_p=400 kHz. Then, when defining the pulse-to-pulse overlap as

$$OL = \left(1 - \frac{v}{d \cdot f_p}\right) \times 100\% \qquad (2)$$

where d [m] denotes the spot diameter. Then, with a beam diameter of 15.6 µm, these parameters imply a OL of 94%. The pulse energy, as well as the number of overscans (or repetitions) N, were varied to study the effect of these parameters on the dimensions (width, depth and edge angle) of the trenches. The pulse energy was varied between 0.25 and 1 µJ and the number of overscans was varied from N=1 to 25. The dimensions of the trenches were determined by CLSM, see Figure 3. As can be observed from Figure 3a and 3b, the trench width and depth increase more or less linear with the number of overscans and the pulse energy. The track width ranges from about 15 µm to 23 µm, whereas the track height varies from 1 µm to 20 µm. The latter is close to the thickness of the PI foil. Figure 3c shows that the edge angle α decreases with increasing number of overscans and increasing pulse energy. Careful analysis of the dependency of the edge angle on the number of overscans at a pulse energy of 1 µJ, shows a discontinuous drop in edge angle from about α=140º to 95º, when the number of overscans is increased from N=3 to 4.

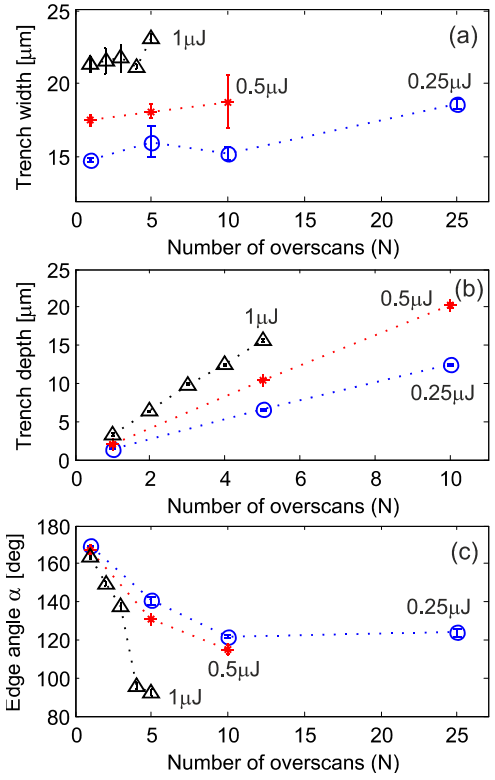

Fig. 3 Dimensions, obtained by CLSM, of single laser tracks (trenches) in PI as a function of number of overscans N and pulse energy. Beam velocity 400 mm/s, pulse frequency 400 kHz. Each data point is an average of 4 measurements.

To explain this result, cross sections of trenches, at a pulse energy of 1µJ as a function of number of overscans were derived from CLSM measurement, see Figure 4b. As can be observed from these cross sections, the edges are "smooth" for overscans up to N=3. That is, the sides of the trench show a gradual change from the unprocessed surface to the center of the trench. For N=4 and 5 the edges show a characteristic "dent" and "hump". The humps show steep edge angles, as small as 92º, which provide a suitable geometrical feature to stop the advancing of the liquid [8].

Similar dents and humps have been previously reported in nanosecond and picosecond UV-laser ablation of PI [14-16]. These studies attribute the humps to a volume increase due to two mechanisms:

i. amorphization (random coiling) of crystalline domains and,
ii. (thermal and non-thermal) fragmentation of polymer chains.

It is worthy to mention that with polymers, hydrodynamic motions are hindered because of high viscosity of melts [17]. And that, with thermostable polymers as polyimide ablation crater does not exhibit residue of melting [18].

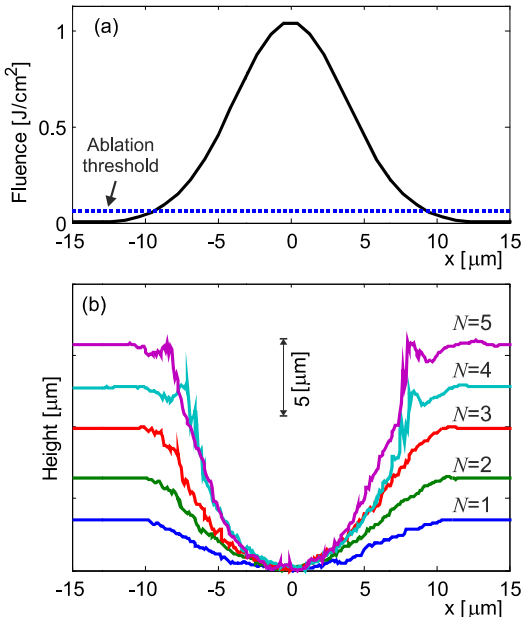

Fig. 4 (a) Laser fluence profile at a pulse energy of 1µJ, (b) Cross sections, obtained by CLSM, of single laser tracks (trenches) in PI as a function of number of overscans *N* at a pulse energy of 1µJ, v=400 mm/s, f_p=400 kHz. Each cross section is an average of 4 measurements.

Dent formation is explained by relaxation of preexistent internal stresses. This mechanism would cause shrinking of the PI, when the surface reaches temperatures high enough for plastic deformation. According to the single pulse experiments of Piglmayer et al. [15], dent and hump formation can occur when the (local) laser fluence is about 70% to 100% of the ablation threshold fluence of the material. Indeed, when comparing Figure 4a to 4b, it can be concluded that, the humps occur near the ablation threshold of the Gaussian fluence profile. It should be noted however, that the features in Figure 4b appear only after exposing areas to multiple overlapping pulses, in contrast with the single shot experiments by Piglmayer et al. Further, Himmelbauer et al. [14] as well as Piglmayer et al. applied relatively long pulse durations of 140 ns up to 50 ms, when compared to the pulse duration of 6.7 ps which was applied to create the features in Figure 4b. An incubation effect, responsible for the growth of dents and humps after successive 6.7 ps laser pulses, might provide an explanation for the surface features shown in Figure 4b. Further research would be required to confirm this.

Anyhow, the humps are constant along edge of the trench and show a very sharp edged side. Those sharp edges provide an excellent pinning location for an advancing front of liquid of receptor sites.

4.3 Machining receptor sites

Receptor sites of approximately 200×200 µm² were created in the PI, using processing conditions discussed in the previous subsection. In addition to the above conditions, receptor sites were created additional overscans equal to N= 6 and 7. Figure 5a shows the strategy/trajectory of the laser spot around the site to create a site. That is, four trenches (obtained by a N overscans of a single laser track) close to the receptor site, were machined at the conditions discussed above. Next, along each side, an area of tracks was machined with a lower number of overscans. These areas allowed an occlusion-free observation of a droplet on the site from the side(s) when using the microscope in the setup as described in section 3.4. For successful application of fluidic self-alignment of receptor sites these areas are not required.

The dimensions (depth and edge angle) of the trench surrounding the sites were measured from CLSM measurements, see Figure 6. It was made sure that the edge angle of the hump (only) was determined, as it is this part of the edge which will stop a fluidic from advancing from the site.

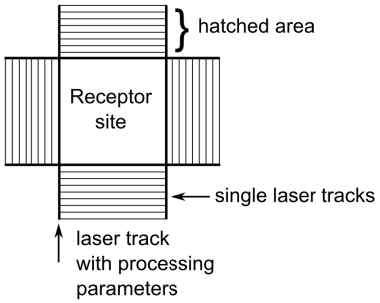

(a)

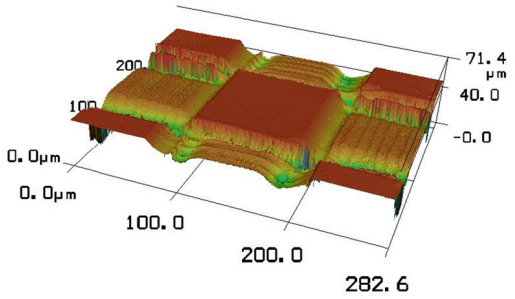

(b)

Fig. 5 (a) Strategy/trajectory of the laser spot to create a receptor site, (b) Isometric representation of a CLSM measurements of a typical receptor site of 100×100 µm².

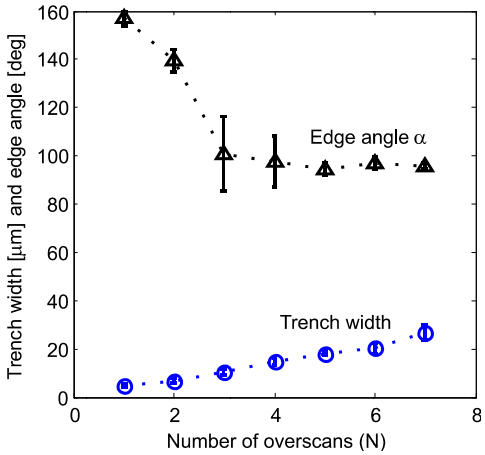

Fig. 6 Dimensions, obtained by CLSM, of trenches surround receptor sites as a function of number of overscans *N* and pulse energy 1µJ, v=400 mm/s and pulse frequency of f_p=400 kHz. Each data point is an average of 8 measurements.

4.4 Liquid confinement measurements

DI water was dispensed onto the receptor site, with increments of tens of picoliters, until it overflowed the edges of the receptor site. Figure 7 shows a typical image of a droplet confined (pinned) on a receptor site, obtained by one of the microscopes as described in section 3.4. The maximum volume of the droplet which could be pinned to a receptor site, just before overflowing, was calculated from these images. That is, the volume can be calculated by using the known receptor area dimensions ($200\times200\mu m^2$) and assuming the shape of the droplet is a spherical cap. This is a valid assumption, as the dimensions of these droplets are far smaller than the capillary length of water. Figure 8 shows the maximum volume of droplets which could be confined to receptor sites with varying edge angle. The graph shows that with reducing edge angle α (sharper edges), the amount of liquid that can be constrained on a site increases. This is in accordance with Gibbs' condition as discussed in section 1.

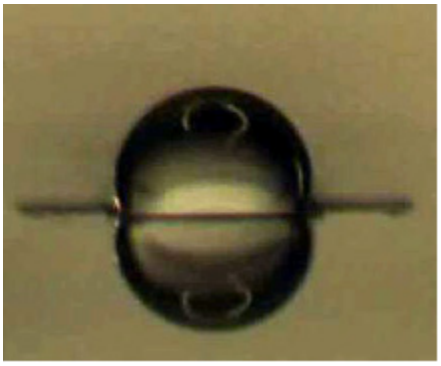

Fig. 7 Side view of a droplet of DI water on a $200\times200\mu m^2$ receptor site. Besides the droplet, also its reflection can be observed.

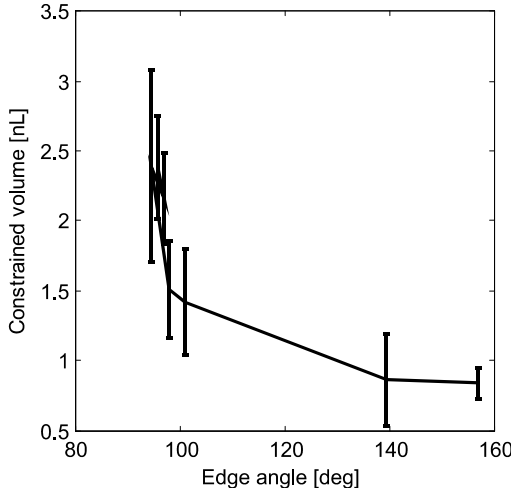

Fig. 8 Maximum volume of the droplet which could be confined on a receptor site as a function the edge angle α of the site.

4.5 Self-alignment tests

Self-alignment tests, using the set-up described in section 3.4, were performed on receptor sites each with different edge angles, as discussed in the previous subsection. And 50 µm thick SU-8 chips of $200\times200\mu m^2$ were used as test parts to be aligned. The polymer SU-8 is an epoxy-based photoresist, which was chosen here for its transparency to visual light. The latter allows access of the position accuracy of the SU-8 chip the receptor site after alignment.

The experiment comprised of the following five steps:

i. the chip is moved to a predefined releasing position near the receptor site,
ii. a droplet of water is dispensed on the site (see Figure 9a),
iii. the chip is released on it (see Figure 9b),
iv. then the chip aligns itself (successfully or unsuccessfully) to the site (see Figure 9c),
v. after a few seconds, water vaporizes, leaving the chip on the receptor site (see Figure 9d).

The performance self-alignment of the SU-8 chip was verified 11 times for each site. All sites showed a 100% success rate of self-alignment, except the sites with the largest edge angles of 156º and 139.4º, which showed a success rate of only 0% and 54.6% respectively. The failing of self-alignment on these sites was found to be due to the water overflowing the receptor site before or during self-alignment. In the case of the site with edge angle of 156º, the droplets were found to overflow the edge during step (*ii*) of the experiment. This can be attributed to the fact that, the droplets are shot at the receptor site at an angle, which implies that its momentum might drive it off the site. In the case of site with an edge angles of 139.4º, the advancement of the droplet was successfully stopped by the edges of the receptor site in some of the experiments. It was found that the receptor sites, showing edges with humps showed a 100 % success rate. These edges were successful at stopping the advancement of the droplet on the site after dispensing.

It was shown in section 4.4 that, the volume of liquid that can be confined on a receptor site is correlated to the edge angle of the site. However, these self-alignment experiments do not show a clear relationship between the edge angle and the success rate of self-alignment. For example, the receptor site with an edge angle of 139.4º was able to confine a water droplet of 0.86 nL (see Figure 8), but during self-alignment experiments the same receptor site was not able to constrain even droplets as small as 0.30 nL at all times, either when dispensed or when the chip was dropped onto the droplet. This shows that the dynamics of self-alignment procedure should be taken into account when determining whether or not a receptor site allows successful self-alignment. Nevertheless, there seems to be a minimum required edge angle for a successful self-alignment.

The final positional and rotational errors of the chip were determined from the top view camera (Figure 9d). The positional misalignment was found to be 0.25±0.86 µm, whereas the rotational misalignment was found to be 0.35±1.22 º. It should be noted however that the resolution of the camera was too low to allow (more) accurate measurements.

5. Conclusions

A ps laser, operating at 343nm wavelength, 400kHz, with a focus diameter of 15.6 µm was used to create receptor sites of 200×200 μm^2 in polyimide foil. Near the edges of the sites, "dents" and "humps" were found showing

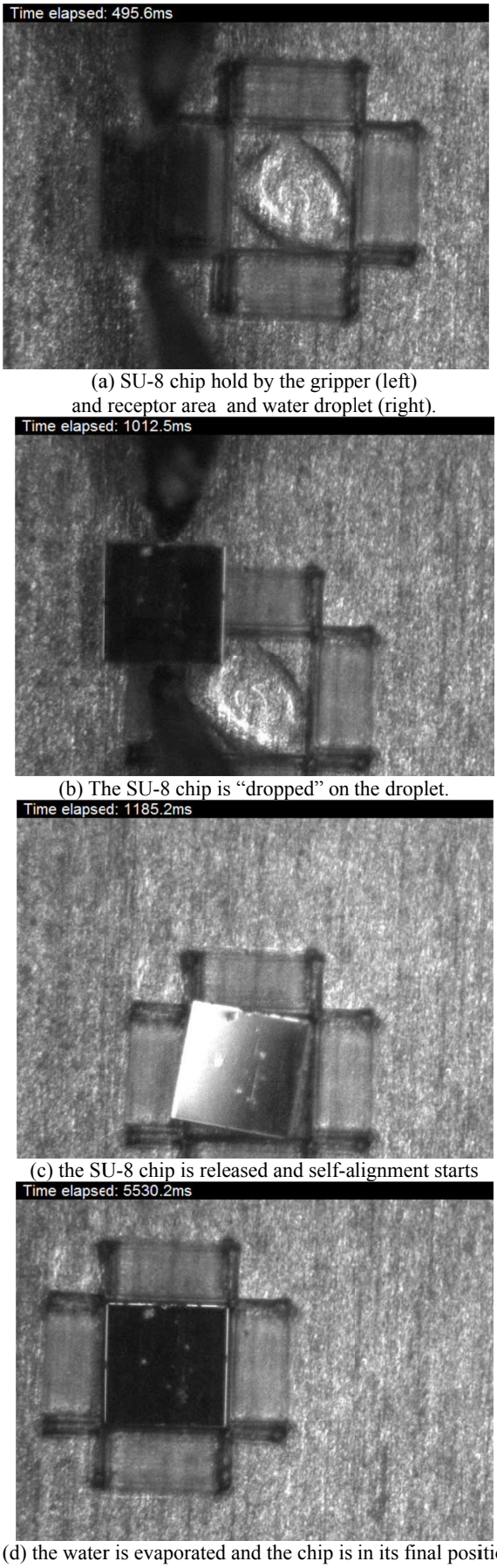

(a) SU-8 chip hold by the gripper (left) and receptor area and water droplet (right).

(b) The SU-8 chip is "dropped" on the droplet.

(c) the SU-8 chip is released and self-alignment starts

(d) the water is evaporated and the chip is in its final position.

Fig. 9 Typical example of frames taken from a video recording of te alignment of an SU-8 chip on a receptor site.

steep edge angles up to about 95º. These edge features provide a suitable geometrical feature to stop the advancing of the liquid which drives self-alignment. It was found, by video based optical contact angle measurement, that the volume of water that is pinned on the receptor site increases with increasing angle of the edges of the receptor site. In addition, it was found, by using a robotic micro-assembly system, that the success rates of self-alignment SU-8 parts on the receptor sites is 100% if the angle of the edges of the receptor site are sharp, due to the dents and humps. The final positional and rotational errors of the chip were found equal 0.25±0.86 μm and 0.35±1.22 º respectively.

Acknowledgments

The authors would like to acknowledge the financial support of the European Union Seventh Framework Programme FP7-2010-NMP-ICT-FoF under Grant Agreement Nº. 260079 - *Efficient and Precise 3D Integration of Heterogeneous Microsystems from Fabrication to Assembly*. http://www.fab2asm.eu.

References

[1] K.F. Böhringer, U. Srinivasan, R.T. Howe, Modeling of capillary forces and binding sites for fluidic selfassembly, Proceedings of the International Conference on Micro Electro Mechanical Systems (MEMS'01), pp. 369-374, (2001).

[2] V. Sariola, M. Jääskeläinen, Q. Zhou, Hybrid Microassembly Combining Robotics and Water Droplet Self-Alignment, IEEE Transactions on Robotics, 26(6), pp. 965 – 977, (2010).

[3] S.H. Liang, X. Xiong, K.F. Böhringer, Towards optimal designs for self-alignment in surface tension driven micro-assembly, Proceedings of the 17th IEEE International Conference on. (MEMS) Micro Electro Mechanical Systems, pp. 9-12, (2004).

[4] V. Sariola, Q. Zhou, H.N. Koivo, Three dimensional hybrid microassembly combining robotic microhandling and self-assembly, 2009 IEEE International Conference on Robotics and Automation, (2009).

[5] V. Sariola, Q. Zhou, R. Laass, H.N. Koivo, Experimental study on droplet based hybrid microhandling using high speed camera, 2008 IEEE/RSJ International Converence on Intelligent Robots and Systems, (2008).

[6] G.R.B.E. Römer, M.M.J. Jorritsma, , D. Arnaldo del Cerro, B. Chang, V. Liimatainen, Q. Zhou and A.J. Huis in 't Veld, Laser micro-machining of hydrophobic-hydrophilic patterns for fluid driven self-alignment in micro-assembly, Proceedings of the 12th International Symposium on Laser Precision Microfabrication, LPM2011, June 7-10, Takamatsu, Japan (2011).

[7] J.W. Gibbs. Scientific Papers Vol. 1, Longmans, London (1906), p. 326 (Dover reprint, New York, 1961).

[8] J. F. Oliver, C. Huh, S. G. Mason, Resistance to spreading of liquids by sharp edges, Journal of Colloid and Interface Science 59 (3) (1977) 568–581.

[9] T. Young, T, An Essay on the Cohesion of Fluids. Philosophical Transactions of the Royal Society of London 95: 65-87 (1805).

[10] X.M. Li, D. Reinhoudt, M. Crego-Calama, What do we need for a superhydrophobic surface? A review on the recent progress in the preparation of superhydro-

phobic surfaces, Chemical Society Reviews 36 (8) 1350–1368 (2007).
[11] J. Bonse, J.M. Wrobel, J. Krüger, and W. Kautek. Ultrashort-pulse laser ablation of indium phosphide in air. Applied Physics A, 72(1):89–94, 2001.
[12] J. Bonse, S. Baudach, J. Krüger, W. Kautek, and M. Kenzner. Femtosecond laser ablation of siliconmodification thresholds and morphology. Applied Physics A, 74(1):19–25, 2002.
[13] Y. Jee, M.F. Becker, and R.M. Walser. Laser-induced damage on single-crystal metal surfaces. Journal of the Optical Society of America B., 5(3):648–658 (1988).
[14] M. Himmelbauer, E. Arenholz, D. Bäuerle, and K. Schilcher. UV-laser-induced surface topology changes in polyimide. Applied Physics A, 63:337–339 (1996).
[15] K. Piglmayer, E. Arenholz, C. Ortwein, N. Arnold, and D. Bäuerle. Single-pulse ultraviolet laser-induced surface modification and ablation of polyimide. Applied Physics Letters, 73:847–849 (1998).
[16] A.A. Serafetinides, C.D. Skordoulis, M.I. Makropoulou, and A.K. Kar. Picosecond and subpicosecond visible laser ablation of optically transparent polymers. Applied Surface Sciences, 135:276–284 (1998).
[17] N. Bityurin, B. S. Luk'yanchuk, M. H. Hong, and T. C. Chong. Models for Laser Ablation of Polymers. Chemical Reviews, 103(2): 519-552 (2003).
[18] D. Bäuerle, Laser Processing and Chemistry, 4th edition, Springer, Heidelberg (2011).